AFRL-AFOSR-UK-TR-2014-0005

Wall-based Actuation for Transition Delay and Drag Reduction

Tamer Zaki

I C Consultants Limited
58 Prince's Gate, Exhibition Road
London, SW7 2PG
UNITED KINGDOM

EOARD SPC 11-4002

Report Date: February 2014

Final Report from 01 September 2011 to 31 August 2013

Air Force Research Laboratory
Air Force Office of Scientific Research
European Office of Aerospace Research and Development
Unit 4515, APO AE 09421-4515

REPORT DOCUMENTATION PAGE

Form Approved OMB No. 0704-0188

1. REPORT DATE *(DD-MM-YYYY)*	2. REPORT TYPE	3. DATES COVERED *(From – To)*
2 February 2014	Final Report	1 September 2011 – 31 August 2013

4. TITLE AND SUBTITLE

Wall-based Actuation for Transition Delay and Drag Reduction

5a. CONTRACT NUMBER

FA8655-11-M-4002

5b. GRANT NUMBER

SPC 11-4002

5c. PROGRAM ELEMENT NUMBER

61102F

6. AUTHOR(S)

Tamer Zaki

5d. PROJECT NUMBER

5d. TASK NUMBER

5e. WORK UNIT NUMBER

7. PERFORMING ORGANIZATION NAME(S) AND ADDRESS(ES)

I C Consultants Limited
58 Prince's Gate, Exhibition Road
London, SW7 2PG
UNITED KINGDOM

8. PERFORMING ORGANIZATION REPORT NUMBER

N/A

9. SPONSORING/MONITORING AGENCY NAME(S) AND ADDRESS(ES)

EOARD
Unit 4515
APO AE 09421-4515

10. SPONSOR/MONITOR'S ACRONYM(S)

AFRL/AFOSR/IOE (EOARD)

11. SPONSOR/MONITOR'S REPORT NUMBER(S)

AFRL-AFOSR-UK-TR-2014-0005

12. DISTRIBUTION/AVAILABILITY STATEMENT

Distribution A: Approved for public release; distribution is unlimited.

13. SUPPLEMENTARY NOTES

14. ABSTRACT

Subjecting a boundary layer to sudden or changing strain can have a profound effect on the flow. In turbulent boundary layers, oscillating the wall has been shown in previous studies as a viable mechanism to reduce drag. At lower Reynolds numbers, and in particular in the transition regime, the flow response is complex. On the one hand, the three dimensionality of the base state can lead to new instabilities. On the other hand, the streaks which are often observed in bypass transition can be weakened, akin to observations in fully-turbulent shear flows. This work investigates the influence of spanwise wall oscillation on bypass transition in zero-pressure-gradient boundary layers. Direct numerical simulations are performed in order to examine the impact of the wall forcing on the non-linear transition process. The simulations demonstrate that appropriate choice of the oscillation amplitude and frequency can delay transition. The non-linear computations are complemented by linear analysis of a simple model that explains the influence of the unsteady shear on the penetration of free-stream vortical disturbances into the boundary layer. This effect, and the weaker streaks in the pre-transitional flow, ultimately lead to a delay in the secondary instability of the streaky base flow and a downstream shift in transition onset.

15. SUBJECT TERMS

EOARD, wall-based actuation, drag reduction, transition delay

16. SECURITY CLASSIFICATION OF:			17. LIMITATION OF ABSTRACT	18, NUMBER OF PAGES	19a. NAME OF RESPONSIBLE PERSON
a. REPORT	b. ABSTRACT	c. THIS PAGE			Gregg Abate
UNCLAS	UNCLAS	UNCLAS	SAR	21	19b. TELEPHONE NUMBER *(Include area code)* +44 (0)1895 616021

Wall-based Actuation for Transition Delay and Drag Reduction

Contract FA8655-11-M-4002*

Final report
December 2013

*This report was prepared in fulfillment of the final requirement for award FA8655-11-M-4002, by T. A. Zaki (t.zaki@imperial.ac.uk) and M.J.P. Hack.

Contents

List of Figures

Wall-based Actuation for Transition Delay and Drag Reduction

Abstract

Subjecting a boundary layer to sudden or changing strain can have a profound effect on the flow. In turbulent boundary layers, oscillating the wall has been shown in previous studies as a viable mechanism to reduce drag. At lower Reynolds numbers, and in particular in the transition regime, the flow response is complex. On the one hand, the three dimensionality of the base state can lead to new instabilities. On the other hand, the streaks which are often observed in bypass transition can be weakened, akin to observations in fully-turbulent shear flows. This work investigates the influence of spanwise wall oscillation on bypass transition in zero-pressure-gradient boundary layers. Direct numerical simulations are performed in order to examine the impact of the wall forcing on the non-linear transition process. The simulations demonstrate that appropriate choice of the oscillation amplitude and frequency can delay transition. The non-linear computations are complemented by linear analysis of a simple model that explains the influence of the unsteady shear on the penetration of free-stream vortical disturbances into the boundary layer. This effect, and the weaker streaks in the pre-transitional flow, ultimately lead to a delay in the secondary instability of the streaky base flow and a downstream shift in transition onset.

1 Introduction

Unsteady wall shear has been shown to effectively reduce turbulent drag in pipe flows, both in numerical simulations and experiments (Quadrio & Sibilla, 2000; Quadrio *et al.*, 2009). These studies have, however, been limited to wall-bounded flows. Investigations of boundary layers are less common in the literature. In addition, none of the previous efforts have considered the influence of wall oscillation on the full process of transition to turbulence in boundary layers. The current work therefore provides the first assessment of the effectiveness of wall actuation on laminar-to-turbulence transition.

Transition mechanisms are generally divided into two classes: The first is known as natural, or orderly, transition and is only observed in controlled environments where the noise level is less than 0.5% of the mean speed. At these low-noise levels, the initial disturbance in a zero-pressure-gradient boundary layer is a Tollmien-Schlichting, linear instability wave. These waves are unstable beyond a critical Reynolds number, $Re_x \simeq 9 \times 10^3$ based on the distance from the leading edge. Full breakdown to turbulence is reached much further downstream at $Re_x \simeq 3 \times 10^6$.

At sub-critical Reynolds numbers, transition to turbulence can take place in presence of appreciable background noise levels. In this case, the breakdown to turbulence is termed bypass transition, because it bypasses the orderly route and Tollmien-Schlichting waves (for a recent review, see Durbin & Wu (2007); Zaki (2013)). The bypass process can be viewed as a three-stage process: Firstly, free-stream vortical disturbances penetrate the boundary layer shear. Secondly, those disturbances which penetrate the shear lead to the amplification of boundary layer streaks, or Klebanoff modes. The streaks are streamwise-elongated regions of high amplitude velocity perturbation. The final stage is marked by the secondary instability and non-linear break-

down of the streaks into turbulent patches. An effective strategy to delay transition to turbulence can attempt to disrupt at least one of the three stages.

The first stage of bypass transition concerns the mechanism whereby free-stream disturbances penetrate the shear. In the inviscid limit, the entire spectrum of free-stream perturbations decays exponentially at the edge of the boundary layer. This filtering process was attributed to the shear by Hunt & Carruthers (1990); Hunt & Durbin (1999), and the term shear sheltering has been used to describe the effect. At finite Reynolds numbers, the boundary layer appears to act as a low-pass filter: While the free-stream disturbance is broadband, the disturbances inside the shear are primarily low frequency. A number of studies have attempted to explain this phenomenology (Jacobs & Durbin, 1998; Zaki & Saha, 2009). The study by Zaki & Saha (2009) provides a physical explanation: Free-stream vortical disturbances convect at the free-stream speed relative to an observer inside the shear. During the characteristic diffusion time, the observer experiences the influence of a number of waves that overtake him. When this number is much less than unity, the observer can in fact "resolve" the free-stream disturbance. This is the case when the free-stream disturbance is low frequency. On the other hand, for high-frequency disturbances, many waves overtake the observer in a diffusive timescale. The net effect, or average, therefore vanishes and high-frequency disturbance are hence filtered, or un-resolved, due to the shear. The model problem was based on the Orr-Sommerfeld operator, and the competition between the shear and viscous diffusion.

Low-frequency perturbations inside the boundary layer amplify to appreciable amplitudes, and are termed streaks due to their elongated appearance. They have also been known as Klebanoff modes – a terminology due to Morkovin & Obremski (1969) in recognition of earlier experimental contributions (Klebanoff, 1971). The mechanism for the amplification of streaks is well established in the literature (Phillips, 1969; Landahl, 1980). A physical interpretation was provided by Schmid & Henningson (2000): The wall-normal displacement, or *lift up*, of the mean flow leads high amplitude streaks. The work by Zaki & Durbin (2005, 2006) provided an alternative view: A three-dimensional vertical velocity perturbation within the boundary layer decays monotonically at sub-critical Reynolds numbers. However, it resonantly forces the generation of a wall-normal vorticity response, which in the low-frequency limit has the appearance of streaks. Linear optimization over all possible initial disturbances demonstrates that a streamwise vortex is most effective at generating streaks (Butler & Farrell, 1992; Schmid & Henningson, 2000; Andersson *et al.*, 1999). The optimization also predicts the spanwise size of the vortex to be on the order of the boundary layer thickness, which matches the observation of naturally occurring streaks in boundary layers beneath free-stream turbulence.

The role of streaks in breakdown to turbulence was not entirely evident in the early literature. Empirical observations suggested that low-speed streaks become unstable when they are lifted towards the edge of the boundary layer. There, the streaks are buffeted by the high-frequency disturbances in the free stream, become unstable and breakdown to turbulence (Jacobs & Durbin, 2001). Another mechanism that is initiated near the wall was reported by Nagarajan *et al.* (2007). These descriptions of breakdown mechanisms, based on direct numerical simulations, were also affirmed by a number of experimental observations (Westin *et al.*, 1994; Matsubara & Alfredsson, 2001; Nolan *et al.*, 2010; Mandal *et al.*, 2010). In addition, streak identification and

tracking techniques have demonstrated that only the highest amplitude streaks host the onset of turbulent spots (Nolan & Zaki, 2013). Secondary instability analysis has provided a theoretical explanation of the influence of streaks on the flow stability. Andersson *et al.* (2001) performed inviscid stability analysis of streaky boundary layers. His base state was computed from direct numerical simulations of the boundary layer response to linearly-optimal, steady streaks. The resulting sinuous and varicose modes were examined, and the threshold for instability was recorded at a critical streak amplitude on the order of 27% of the free-stream speed. Vaughan & Zaki (2011) subsequently performed viscous analysis of streaky boundary layers. His base state was obtained from direct numerical simulations of the boundary layer response to inflow free-stream modes. Therefore, the base state streaks were unsteady, but nonetheless repeated in the span at a fundamental wavenumber. The analysis by Vaughan & Zaki (2011) led to an interesting discovery. The streaky boundary layer has two modes of instability: An outer mode which is related to the instability of lifted low-speed streaks which were described by Jacobs & Durbin (2001); An inner mode, whose critical layer is near the wall, and which explains the observations by Nagarajan *et al.* (2007). Most recently, Hack & Zaki (2014) examined the stability of streaky boundary layers beneath broadband free-stream turbulence. The base state was therefore more realistic than any previous study: a boundary layer with a large number of streaks, all with different shapes, orientations and amplitudes. Hack & Zaki (2014) demonstrated that their analysis can identify the particular streak that becomes unstable and hosts the onset of turbulence. Each such event leads to the formation of a turbulence spot, and these patches spread and merge to form the fully-turbulent boundary layer.

In this work, the influence of spanwise wall oscillation on the above progression of event, and the bypass process, is examined. A discussion of the influence of the spanwise shear on the penetration of free-stream vortical disturbances into the boundary layer is provided. In addition, using direct numerical simulations, the impact on the full non-linear problem is studied. This includes the influence of the wall forcing on the amplification of streaks, their breakdown to turbulence, and the formation of the fully-turbulent boundary layer downstream.

2 Direct numerical simulations

A schematic of the computational domain for the direct numerical simulations is shown in figure 1. The dashed line in the figure marks the boundary of the simulation domain. It starts at $R_\theta = 80$, downstream of the leading edge. This approach reduced the computational cost that would be required to resolve the leading edge region. However, appropriate boundary conditions are now required in order to represent the free-stream turbulence at this location. The inflow condition adopted in this work is based on the work by Jacobs & Durbin (2001), where synthetic inflow turbulence is expressed as a superposition of eigenmodes of the linear perturbation equations. The inlet free-stream turbulence intensity and lengthscale can be prescribed. Downstream of the inlet plane, the full non-linear Navier-Stokes equations are solved. Therefore, all non-parallel and non-linear effects are fully represented in the simulations of the downstream evolution of the boundary layer.

The size of the simulation domain, normalized by the inlet δ_{99}, is $1200\times30\times40$ in the streamwise, wall-normal, and spanwise directions. The grid resolution is the same as

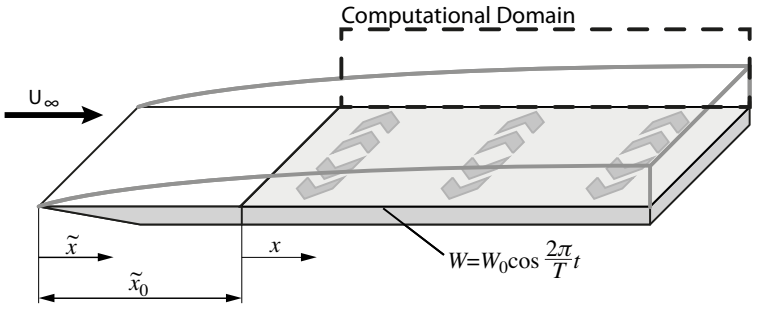

Figure 1: Schematic of the DNS domain. The domain boundary is indicated by the dashed line.

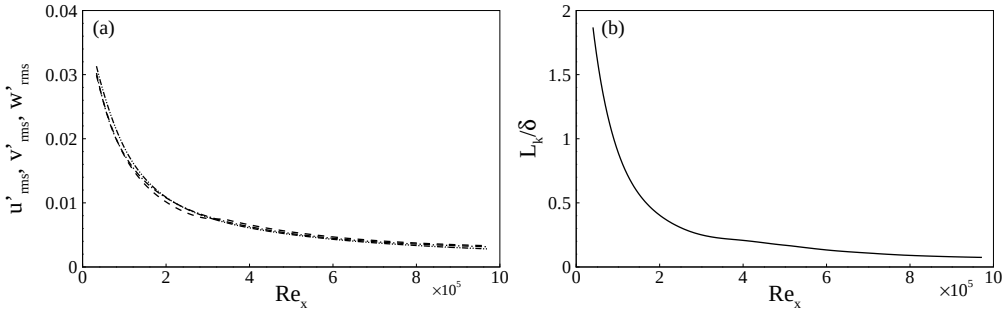

Figure 2: Free-stream decay of turbulence: (a) Rms of the velocity fluctuations u' (dashed), v' (dash-dotted), w' (dash-dot-dotted) versus Reynolds number Re_x; (b) Turbulent length scale L_k normalized by the local boundary layer thickness δ versus Reynolds number Re_x.

that adopted by Jacobs & Durbin (2001) who performed an extensive grid refinement study for simulation of bypass transition. In order to ensure zero-pressure-gradient in the streamwise direction, a suction velocity is applied at the top of the domain in order to make up for the growth of the boundary layer. Periodicity is enforced in the spanwise direction, and a convective outflow condition is applied at the exit boundary of the domain. At the bottom wall, no-slip and no-penetration conditions are applied to the streamwise, u, and wall-normal, v, components of the velocity vector. The spanwise component is subjected to a harmonic motion, $w(y = 0) = W_0 \sin(2\pi t/T)$. The oscillation of the bottom wall is assumed to start at the inlet of the computation domain, and that the flow upstream follows the Blasius solution.

In bypass transition, it is important to characterize the free-stream turbulence. Two main quantities that dictate the transition location inside the boundary layer are the free-stream turbulence intensity, T_u and the lengthscale, L_k. These two quantities are plotted in figure 2 versus the downstream Reynolds number. It is seen that the free-stream turbulence decays from an inflow value of approximately 3%, and the turbulence lengthscale is approximately 2δ at the inlet. In figure 2, the lengthscale is normalized by the local boundary layer thickness, and hence appears to decay because the increase in $\delta(x)$ is faster than the growth of L_k.

Since the base flow in the current simulations is time dependent, it is important to

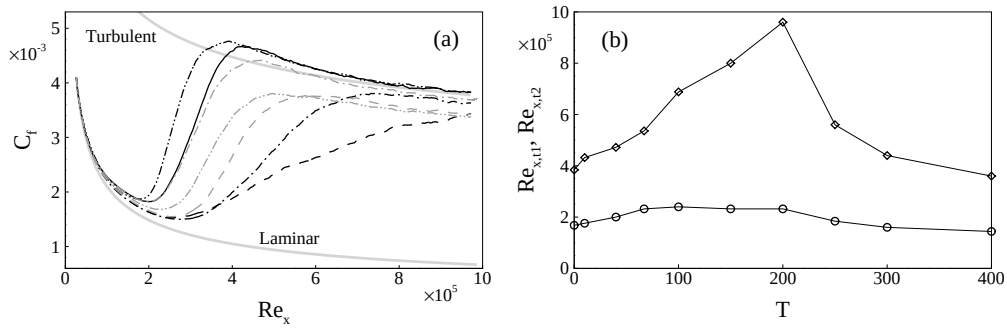

Figure 3: (a) Skin friction coefficient in the (solid) reference simulation and with wall oscillation, $W = 0.25$. The oscillation periods considered are (gray dash-dotted) $T = 10$; (gray dashed) $T = 40$; (gray dash-dot-dotted) $T = 67$; (black dash-dotted) $T = 100$; (dashed) $T = 200$; and (dash-dot-dotted) $T = 400$; (b) Reynolds number at onset and end of transition, $Re_{x,\,t1}$ and $Re_{x\,t2}$ respectively.

introduce the triple decomposition,

$$a = \overbrace{\bar{a} + \tilde{a}_\phi}^{\langle a \rangle_\varphi} + a' \tag{1}$$

where $\bar{a}$ is the spanwise- and time-average, $\tilde{a}_\varphi$ is the time-periodic component, and a' is the stochastic fluctuation. The term $\langle a \rangle_\varphi$ is the phase average, where φ is determined by the phase of the wall oscillation.

A summary of the outcome of the DNS is given in figure 3, where the skin friction is plotted versus the downstream Reynolds number. The reference curve shows that transition onset is near $Re_x = 2 \times 10^5$. When the wall oscillation is introduced, the transition location changes, and also the transition length is altered. All the curves are at the same amplitude of wall oscillation, $W_0 = 0.25$. As the period of oscillation is increased from $T = 10$ to $T = 200$, the transition onset location moves downstream and the transition length is extended. At $T = 400$, the transition onset is suddenly shifted upstream of the reference case. Figure 3 in the right panel shows the Reynolds number at the start and end of transition.

A comparison of the perturbation field inside the reference simulation and the optimal case ($W_0 = 0.25$, $T = 200$) is provided in figure 4. The top views show the streamwise stochastic perturbation velocity, u'. It should be noted that the length of the two panels are different. In the top panel, the reference simulation captures the well-established stages of bypass breakdown: Only low-frequency disturbances are observed inside the boundary layer. These streaks reach high amplitude, and become host for the onset of localized turbulence patches. Fully-turbulent flow is observed near $x = 400$. In the case with wall oscillation, the perturbation field is much less energetic, and elongated streaks are nearly absent in the pre-transition region. A localized spot inception event is observed near $x = 550$, and fully-turbulent flow is achieved farther downstream, relative to the reference case.

The observations from the instantaneous realizations in figure 4 are supported by the root-mean-square of the perturbation velocity, u'_{rms}, within the boundary layer in figure 5. A comparison of the reference and optimal cases is provided in the figure. In the reference case, the root-mean-square shows amplification of the disturbance inside the boundary layer, near $y/\delta(x) \simeq 0.4$. Further downstream, the location of the

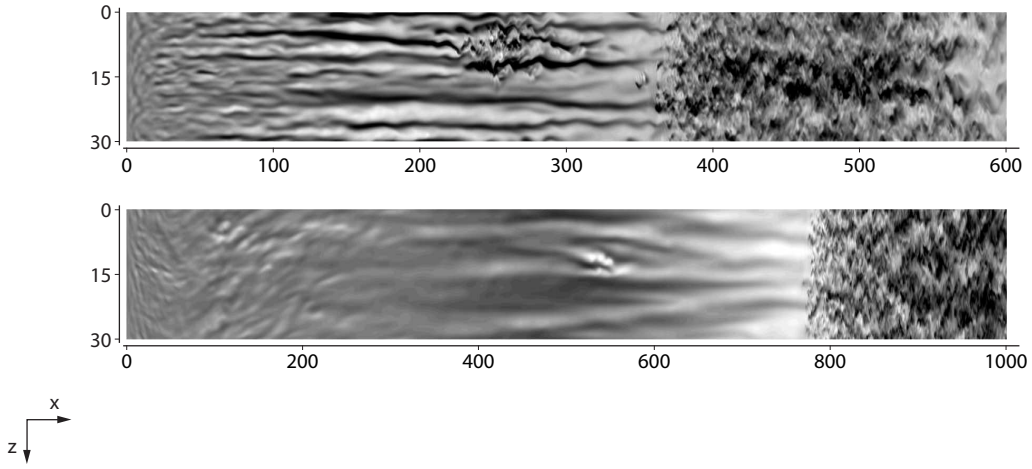

Figure 4: Top views of the streamwise velocity disturbance inside the boundary layer, $|u'| < 0.2$. Top: reference simulations without wall oscillation. Bottom: optimal wall oscillation frequency.

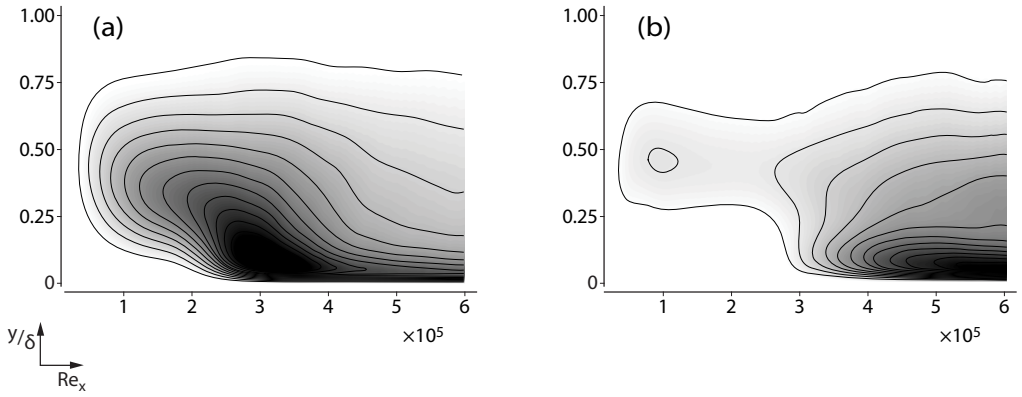

Figure 5: Root-mean-square of the streamwise velocity fluctuations. (a) Reference simulation; (b) Optimal wall oscillation.

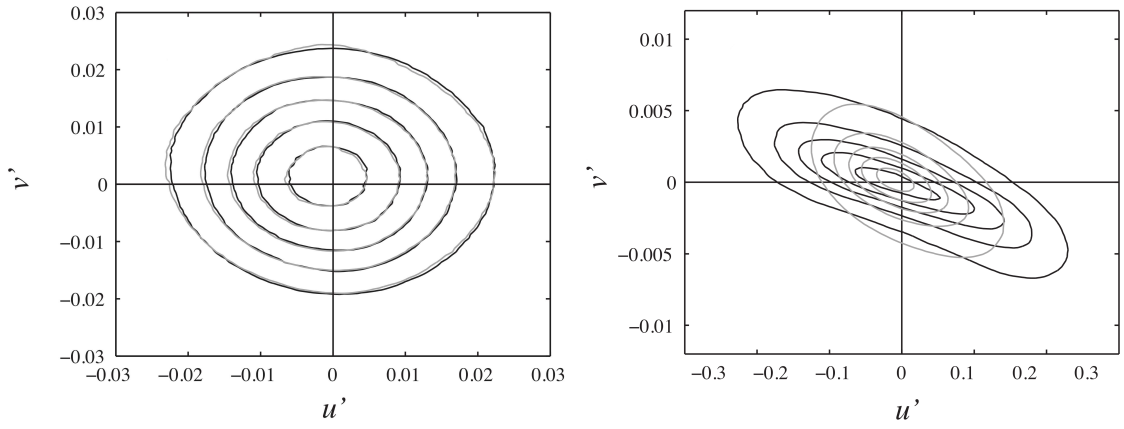

Figure 6: Contours of the joint probability density functions for u' and v'. At left, the joint p.d.f. is evaluated in the free stream and inside the boundary layer at right, $y/\delta = 0.4$. Black: reference simulation; Gray: optimal wall oscillation frequency.

maximum shifts towards the wall. This shift towards coincides with the laminar-to-turbulence transition process. In comparison, the case with wall oscillation is markedly different. The initial energy amplification is substantially reduced. This weaker amplification of the disturbance in the boundary layer is symptomatic of weaker streaks in presence of wall actuation. The disturbance level inside the boundary layer remains weak far downstream of the inlet, relative to the reference case. Near $Re_x \sim 4 \times 10^5$, a sudden shift towards a near-wall maximum is observed.

The reduction in u' can explain the delay in transition. In the canonical bypass scenario, Nolan & Zaki (2013) demonstrated that spot inception is localized on streaks that reach high amplitude, $A_u > 0.2U_\infty$. Furthermore, linear analyses have also shown that the growth rate of the secondary instability of the streaky base state depends on the amplitude of the streaks (Andersson *et al.*, 2001; Vaughan & Zaki, 2011; Hack & Zaki, 2014). As a result, a weaker root-mean-square disturbance in the case of wall oscillation is consistent with a lower likelihood of streak instability and breakdown to turbulence.

The lower streak amplitude in the controlled flow hints to a weakening in the lift-up mechanism, for example due to a smaller wall-normal velocity perturbations inside the shear. A joint probability density function of the (u', v') perturbations is provided in figure 6. In the free stream (left panel), the disturbances are isotropic which leads to the circular shape of the joint probability density function. Inside the shear (right panel), the elongated shape of the contours is indicative of the amplification of the streaks by ejections (second quadrant) and sweeps (fourth quadrant). The figure demonstrates that, inside the boundary layer, the vertical velocity disturbances are generally of lower amplitude in the case where the wall oscillation is active, and the resulting streaks are also lower amplitude than in the reference simulation. In the following section, the influence of spanwise wall oscillation on the eigen-spectrum of the boundary layer is examined. The linear analysis provides a possible explanation of the weakening of the vertical velocity perturbation field.

3 Eigen-spectrum of the linear perturbation equations

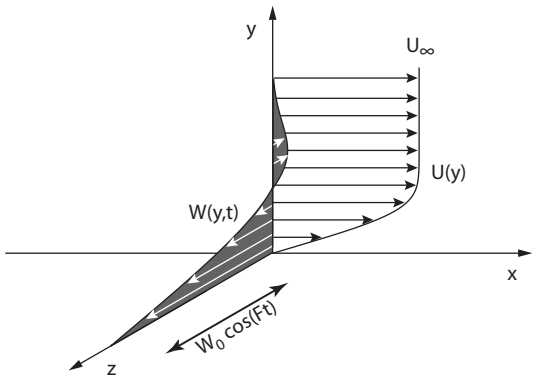

Figure 7: Illustration of the base flow, $\underline{U} = (U, 0, W(y,t))^T$

A schematic of the base flow adopted in this section is shown in figure 7. In addition to the Blasius profile in the streamwise direction, we include a time-harmonic spanwise flow $W(y,t)$ which is a solution to the Stokes second problem. The complete flow is given by,

$$\underline{U} = (U(y), 0, W(y,t))^T .$$

The analytical expression for the spanwise component is given by,

$$W(y,t) = W_0 \exp\left(-\sqrt{\frac{Re\pi}{T}}y\right) \cos\left(\frac{2\pi}{T}t - \sqrt{\frac{Re\pi}{T}}y\right), \tag{2}$$

where the magnitude of the wall speed is W_0 and the period of oscillation is T. In the above expression, and throughout this work, the Reynolds number is based on the streamwise component of the flow, $Re \equiv U_\infty \delta/\nu = 10^3$, where δ is the 99% boundary layer thickness and U_∞ is the Blasius free-stream speed.

The equations which govern the time-evolution of a small perturbation, $\underline{u'} = (u', v', w')^T$, about the above mean flow are derived using standard techniques. First, one assumes the velocity is decomposed into mean and perturbation components $\underline{u} = \underline{U} + \underline{u'}$. The equations that govern $\underline{u'}$ are linearized by neglecting products of perturbations. The final outcome can be cast in a form that resembles the Orr-Sommerfeld equation, for the normal-velocity perturbation,

$$\left[\left(\frac{\partial}{\partial t} + U\frac{\partial}{\partial x} + W\frac{\partial}{\partial z}\right)\nabla^2 - \frac{\partial^2 U}{\partial y^2}\frac{\partial}{\partial x} - \frac{\partial^2 W}{\partial y^2}\frac{\partial}{\partial z} - \frac{1}{Re}\nabla^4\right] v' = 0. \tag{3}$$

Similar to the original Orr-Sommerfeld equation, the coefficient in equation 3 are homogeneous in the streamwise and spanwise directions, and therefore a normal-mode assumption is invoked in those dimensions,

$$v'(x,y,z,t) = v(y,t)\exp(\mathrm{i}k_x x)\exp(\mathrm{i}k_z z). \tag{4}$$

Since we consider a time-harmonic base flow, $W(y,t)$, the perturbation can be expressed as a Floquet expansion in terms of the fundamental frequency $F = 2\pi/T$ of the base

flow,

$$v\left(y,t\right)=\exp\left(\sigma t\right)\sum_{n=-\infty}^{\infty}v_{n}\left(y\right)\exp\left(\mathrm{i}nF\ t\right). \tag{5}$$

In the temporal problem, the exponent $\sigma=\sigma_{\mathrm{r}}+\mathrm{i}\sigma_{\mathrm{i}}$ is the complex eigenvalue, with σ_{r} giving the growth rate and σ_{i} is a frequency shift. The final form of the disturbance equation is therefore,

$$\sum_{n=-\infty}^{\infty}\left[\left(-\mathrm{i}\sigma+nF+k_{x}U+k_{z}W\right)\left(\mathcal{D}^{2}-\kappa^{2}\right)-k_{x}\frac{\partial^{2}U}{\partial y^{2}}-k_{z}\frac{\partial^{2}W}{\partial y^{2}}\right.$$
$$\left.+\mathrm{i}\frac{1}{Re}\left(\frac{\partial^{2}}{\partial y^{2}}-\kappa^{2}\right)^{2}\right]\exp\left(\mathrm{i}\left(-\sigma+nF\right)t\right)v_{n}\left(y\right)=0, \tag{6}$$

with $\kappa^{2}\equiv k_{x}^{2}+k_{z}^{2}$. The eigenvalues of σ are the particular values of the complex frequency that yield solutions of the above system. The solution v_n is the Floquet representation of the eigenfunction v, as described by equation (5). Note that the expression of v_n is not independent of $n\pm1$: if the base flow is time-harmonic, products of $W(y,t)$ and v_n couple each Floquet component n to $n\pm1$. Therefore, the eigenvalue problem becomes a system of coupled equations for all the Floquet components.

The continuous spectrum

In order to study free-stream vortical disturbances, we focus our attention to the continuous spectrum of the disturbance equations. The modes which belong to the continuous branch are obtained by taking the limit $y\to\infty$ of the governing equations. In that limit, the base flow derivatives vanish, and it is possible to obtain an analytical form of the dispersion relation, by assuming that the disturbance is oscillatory in the free stream. Substituting $U=U_{\infty}$ and $W=\frac{\partial^{2}U}{\partial y^{2}}=\frac{\partial^{2}W}{\partial y^{2}}=0$ in equations 6, the disturbance in the free stream is governed by,

$$\left[\left(-\mathrm{i}\sigma+nF+k_{x}U\right)\left(\mathcal{D}^{2}-\kappa^{2}\right)+\mathrm{i}\frac{1}{Re}\left(\mathcal{D}^{2}-\kappa^{2}\right)^{2}\right]v_{n}^{\infty}=0. \tag{7}$$

In the above, n is a parameter and we focus on a particular, yet arbitrary, value $n=\widetilde{n}$. This allows us to solve for the eigenvalue σ, which is shared among all components of the Floquet expansion, and the corresponding eigenfunction is a summation of all the Floquet components. While $v_{n=\widetilde{n}}^{\infty}$, is finite and bounded for the continuous modes, the remaining terms in the expansion, $v_{n\neq\widetilde{n}}^{\infty}$, must vanish in the fee stream in order to satisfy equation7.

The dispersion relation is obtain using $n=\widetilde{n}$ in the above equation,

$$\left[\left(-\mathrm{i}\sigma+\widetilde{n}F+k_{x}U\right)\left(\mathcal{D}^{2}-\kappa^{2}\right)+\mathrm{i}\frac{1}{Re}\left(\mathcal{D}^{2}-\kappa^{2}\right)^{2}\right]v_{\widetilde{n}}^{\infty}=0, \tag{8}$$

and seeking solutions of the form $v_{\widetilde{n}}^{\infty}\left(y\right)=\sum_{j=1}^{4}C_{j}\exp\left(\lambda_{j}y\right)$, where λ_j are the roots of the characteristic given by,

$$\lambda_{1,2}^{2}=\kappa^{2}$$
$$\lambda_{3,4}^{2}=\kappa^{2}+\mathrm{i}Re\left(-\mathrm{i}\sigma+\widetilde{n}F+k_{x}U_{\infty}\right).$$

In order to ensure oscillatory behavior of the eigenfunctions, we set $\lambda_{3,4}^2 = -k_y^2$, where k_y is a real valued parameter, which represents the wall-normal wavenumber of the $n = \widetilde{n}$ Floquet mode. The resulting value of σ is therefore given by the dispersion relation,

$$\sigma = -\mathrm{i}\left(k_x U_\infty + \widetilde{n} F\right) - \frac{1}{Re}\left(k_x^2 + k_y^2 + k_z^2\right). \tag{9}$$

The above relation shows that multiple continuous branches exist. Each branch is traversed by changing the continuous parameter k_y; Furthermore, the branches are separated by the frequency F of the base flow, and each branch is obtained by selecting a different value of $\widetilde{n}$. A schematic of the eigenvalue spectrum of the unsteady base flow is shown in figure 8: discrete modes are shown by circles and the continuous branches are marked by crosses.

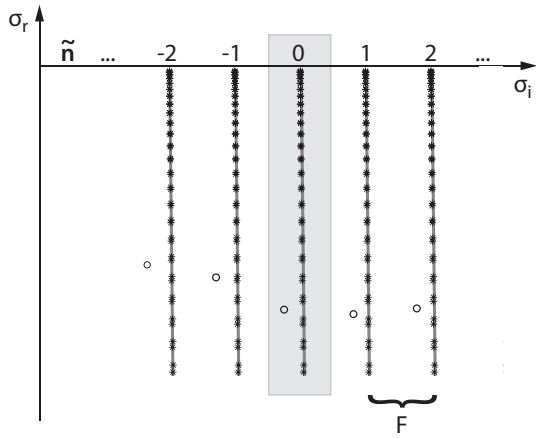

Figure 8: Schematic of the Floquet eigen-spectrum. Eigenvalues of the ($\circ$) discrete and ($*$) continuous spectra.

Once the eigenvalue is computed from equation 9, the eigenfunctions are evaluated as solutions to equation 6. This requires four boundary conditions on v_n, two at the wall and two in the free stream. The no-slip conditions at the wall yield,

$$v_n\left(y = 0\right) = 0, \tag{10}$$

$$\frac{dv_n}{dy}\left(y = 0\right) = 0 \;\forall\; n. \tag{11}$$

In the free stream, only $v_{n=\widetilde{n}}$ satisfies the boundedness condition which, following Jacobs & Durbin (1998), is evaluated at two points y_1 and y_2 in the free stream and has the form,

$$v_{\widetilde{n}}^{\infty} = 1, \tag{12}$$

$$\frac{\left(\mathcal{D}^2 v_{\widetilde{n}}^{\infty} + k_y^2 v_{\widetilde{n}}^{\infty}\right)_{y1}}{\left(\mathcal{D}^2 v_{\widetilde{n}}^{\infty} + k_y^2 v_{\widetilde{n}}^{\infty}\right)_{y2}} = \exp\left(k_y\left(y_2 - y_1\right)\right). \tag{13}$$

All other Floquet components, $v_{n\neq\widetilde{n}}^{\infty}$, vanish in the free stream since they must satisfy equation 7 while σ was obtained using $n = \widetilde{n}$ only.

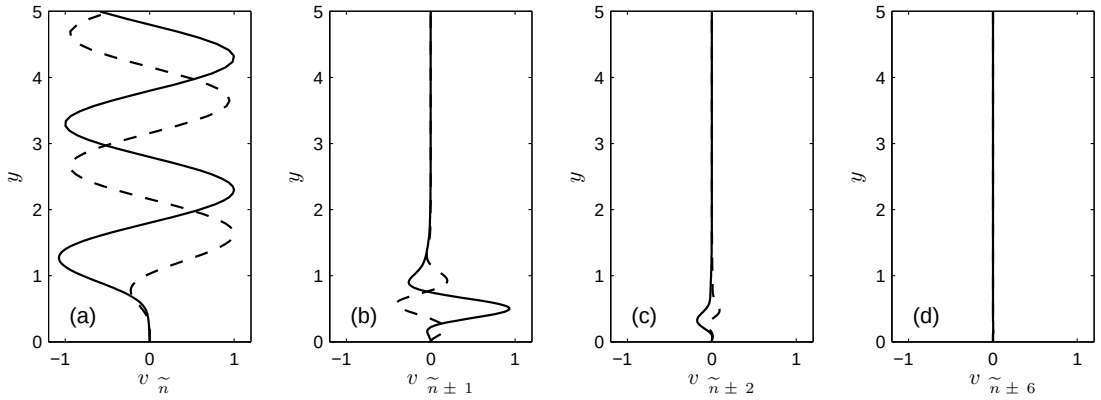

Figure 9: Selected components v_n of the Floquet expansion for $T = 40$, $W_0 = 0.25U_\infty$. (a) $n = \widetilde{n}$; (b) $n = \widetilde{n} \pm 1$; (c) $n = \widetilde{n} \pm 2$; (d) $n = \widetilde{n} \pm 6$; (——) Real component; (– – –) imaginary component

The eigenvalue problem 6 subject to the above boundary conditions is solved using a Chebyshev discretization, using the methodology described by Liu *et al.* (2008*a*,*b*) and Vaughan & Zaki (2011). An example of the Floquet modes for a time-periodic base flow is shown in figure 9. Only the zeroth component, $(\widetilde{n})$, is oscillatory in the free stream while all other Floquet components, $n \neq \widetilde{n}$, vanish in the free stream. Within the boundary layer, only the zeroth and first harmonic, $\widetilde{n}$ and $\widetilde{n}\pm 1$, contribute significantly to the energy within the shear; higher harmonics are relatively inappreciable.

Modal Sheltering

In a streamwise, Blasius boundary layer, low-frequency continuous modes are known to penetrate deepest into the shear (Zaki & Saha, 2009). These elongated disturbances are responsible for the generation of boundary layer streaks, and hence have received a great deal of attention in the literature. Introducing spanwise, unsteady flow can, however, alter the ability of these modes to penetrate the boundary layer. An example is shown in figure 10 where the same low-frequency mode is evaluated in presence of unsteady base flow, $W(y,t)$. As the period of the base flow is increased, the Stokes layer thickness increases and the additional shear enhances the sheltering characteristics of the base flow.

In order to quantify the ability of unsteady wall shear to shelter the boundary layer from free-stream vortical forcing, we introduce a "sheltering parameter", s, where

$$s \equiv \int_0^\delta \frac{v_\infty - v\,(y)}{v_\infty}\,\mathrm{d}y,$$

and v_∞ is the average free-stream amplitude of the eigenfunction. The sheltering parameter, s, tends to zero when the boundary layer is permeable to the free-stream mode and unity when it is perfectly sheltered. Figure 11 shows contours of s over a wide range of wavenumber vector (k_x, k_z) for Blasius flow (without unsteady shear). In the low-frequency limit, or $k_x \to 0$, the boundary layer is susceptible to disturbances and sheltering vanishes. In this limit, sheltering is insensitive to the spanwise wavenumber, k_z.

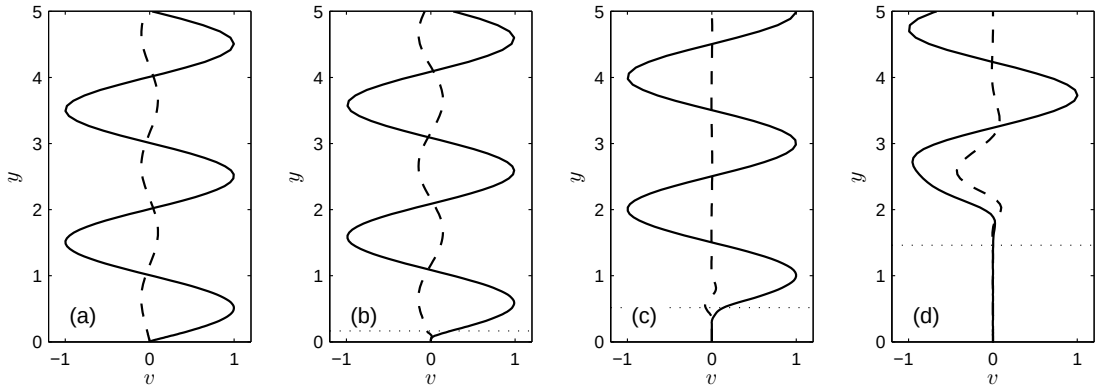

Figure 10: Modal sheltering for (a) Blasius and (b – d) Stokes-Blasius flow. The dotted line marks the thickness of the Stokes layer. $W_0 = 0.25U_\infty$, $T = \{4, 40, 400\}$, $d_{\text{Stokes}}/\delta = \{0.16, 0.52, 1.64\}$; (——) real and (– – –) imaginary components of the eigenfunction.

The influence of unsteady base-flow motion, $W(y,t)$, is shown in figure 12. Sheltering becomes dependent on the spanwise wavenumber, k_z, with enhanced sheltering for large k_z values. In the limit of low wavenumber vector, (k_x, k_z), sheltering is dependent on the ratio of the two wavenumbers, or modal orientation.

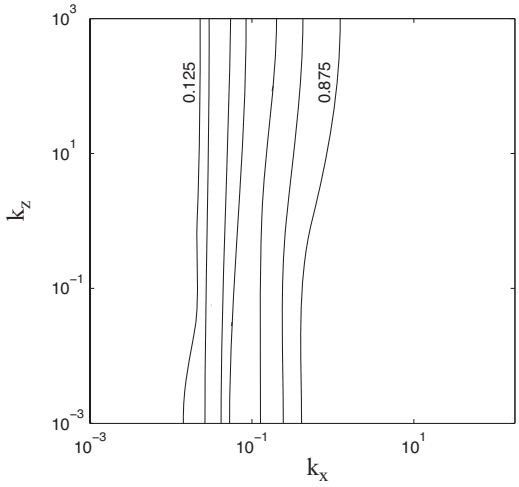

Figure 11: Quantitative evaluation of modal sheltering for Blasius flow; lines denote levels from 0.125 to 0.875 with an increment of 0.125

Energy Sheltering

In order to quantify the ability of spanwise, unsteady motion to enhance shear-sheltering, we evaluate the fraction of free-stream energy that penetrates the boundary layer shear for different parameters of the Stokes-like wall layer. The free-stream turbulence is

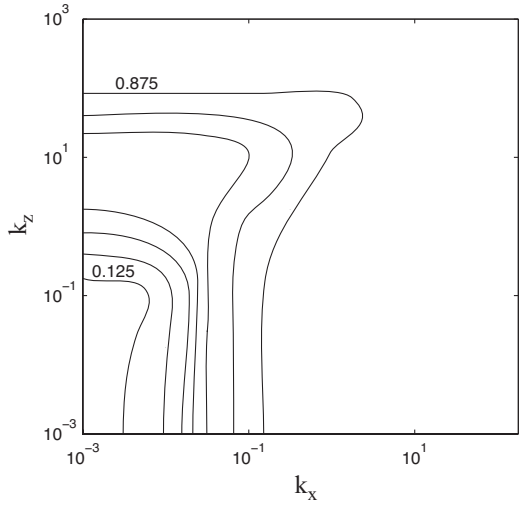

Figure 12: Quantitative evaluation of modal sheltering for combined Stokes-Blasius flow of $T = 100$, $W_0 = 0.25U_\infty$; lines denote levels from 0.125 to 0.875 with an increment of 0.125

modeled using a superposition of continuous Orr–Sommerfeld and Squire modes, following the approach first introduced by Jacobs & Durbin (2001). The turbulence is expanded in terms of Fourier modes in the spanwise and temporal dimensions, and is expanded in terms of continuous-spectrum modes in the wall-normal direction. The latter are oscillatory in the free stream, and therefore resemble a Fourier expansion. As a result, in the free stream, the disturbance behavior is of the form,

$$v' \sim \hat{v} \exp\left(\mathrm{i}\left(k_x x + k_y y + k_z z\right)\right),$$

$$\eta' \sim \hat{\eta} \exp\left(\mathrm{i}\left(k_x x + k_y y + k_z z\right)\right),$$

where $\eta \equiv \partial u/\partial z - \partial w/\partial x$ is the wall-normal vorticity. Note, however, that as the wall is approached, the Orr–Sommerfeld and Squire modes decay in a manner consistent with the linear perturbation equations.

Following the work by Jacobs & Durbin (2001), we adopt the scaling $\hat{v} = -\mathrm{i}A\sqrt{k_x^2 + k_z^2}/k$ and $\hat{\eta} = -\mathrm{i}B\sqrt{k_x^2 + k_z^2}$. Using continuity and the definition of the wall-normal vorticity, the following expressions for the modal coefficients are obtained,

$$\begin{aligned}
\hat{u} =& \frac{\mathrm{i}Ak_xk_y}{k\sqrt{k_x^2 + k_z^2}} + \frac{Bk_z}{k_x^2 + k_z^2}, \\
\hat{v} =& -\mathrm{i}\frac{A\sqrt{k_x^2 + k_z^2}}{k}, \\
\hat{w} =& \frac{\mathrm{i}k_yk_zA}{k\sqrt{k_x^2 + k_z^2}} - \frac{Bk_x}{k_x^2 + k_z^2},
\end{aligned} \tag{14}$$

where $k \equiv \sqrt{k_x^2 + k_y^2 + k_z^2}$. A Von Karman spectrum is assumed (Von Kármán, 1948),

$$E\left(k\right) = \frac{L^5k^4}{C\left(1 + \left(kL\right)^2\right)^{17/6}},$$

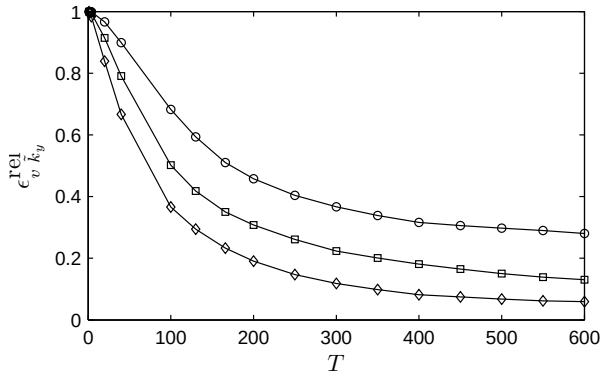

Figure 13: Normalized von Karman-weighted modal energy within the boundary layer for $k_y = \pi$; $\circ$, $W_0 = 0.1U_\infty$; $\square$, $W_0 = 0.2U_\infty$; $\diamond$, $W_0 = 0.4U_\infty$

where $L = \frac{55C}{9\pi}L_{11}$ and $C = 0.6884$. The characteristic lengthscale of the free-stream turbulence is here assumed to be $L_{11} = 1$, i.e. equal to the boundary layer thickness. Furthermore, the total energy, $\int_0^\infty E\left(k\right)\mathrm{d}k = 3/2$. The expressions for A and B are given by,

$$\begin{aligned} A =& \mathcal{F}\exp\left(\mathrm{i}\theta_1\right)\cos\gamma \\ B =& \mathcal{F}\exp\left(\mathrm{i}\theta_2\right)\sin\gamma, \end{aligned}$$

where $\mathcal{F}^2\left(k\right) \equiv E\left(k\right)/\left(2\pi k^2\right)$; the angles θ_1, θ_2 and γ are random and uniformly distributed (Rogallo, 1981).

Since we are primarily concerned with the wall-normal component of the free-stream vortical spectrum, we focus on the expression for the energy contained in $v(\underline{k})$,

$$\rho_v\left(\underline{k}\right) = \frac{1}{2}\frac{E(k)}{4\pi k^2}\frac{k_x^2 + k_z^2}{k^2}.$$

The total energy in the wall-normal velocity is therefore,

$$\epsilon_v = \int_0^\infty \int_0^\infty \int_0^\infty \rho_v\left(\underline{k}\right)\ \mathrm{d}k_x\,\mathrm{d}k_y\,\mathrm{d}k_z = 1/2.$$

We further restrict our results to the case where $\widetilde{k}_y = \pi$, because these modes have a wall-normal characteristic scale on the order of the boundary layer thickness. Smaller disturbance also penetrate the shear, but are viscously damped, while larger disturbances are blocked by the wall. With the assumption, the total energy in $\widetilde{k}_y$ within the shear can be computed from the expression,

$$\epsilon_{v\,\widetilde{k}_y} = \frac{1}{\delta}\int_0^\delta \int_{k_x}\int_{k_z} \rho_v\left(\underline{k}\right)\|v\left(y;\underline{k}\right)\|\mathrm{d}k_z\,\mathrm{d}k_x\mathrm{d}y.$$

In order to compare the penetration of free-stream energy into the shear for cases with wall oscillation relative to the simple Blasius profile, we compute, $\epsilon^{\mathrm{rel}}_{v\,\widetilde{k}_y} \equiv \epsilon_{v\,\widetilde{k}_y}/\epsilon^{\mathrm{Blasius}}_{v\,\widetilde{k}_y}$, which is shown in figure 13. Increasing the period or amplitude of wall oscillation has an adverse effect on the fraction of free-stream vortical disturbance that penetrates

near the wall: Longer periods of oscillation yield a thicker spanwise shear layer, which enhances sheltering away from the wall; Increasing the amplitude of oscillation also increases the level of shear, and hence sheltering.

The wall oscillation, therefore, reduces the total energy that penetrates the boundary layer. The continual change in the direction of the shear also changes the portion of the free-stream spectrum that reaches the near-wall flow (Hack & Zaki, 2012). These results are consistent with the observations from the direct numerical simulations where the v' perturbations were weaker inside the boundary layer in the case with wall oscillation, and the streaks were lower in amplitude in comparison to the reference simulations. The overall impact on transition in the optimal case was a downstream shift in the onset of breakdown to turbulence, and an extended transition length.

4 Conclusions

Bypass transition to turbulence is often divided into three stages. First, external disturbances from the free stream penetrate the boundary layer. Second, these disturbances lead to a boundary layer response, often in the form of amplifying streaks with high streamwise velocity amplitude. The third and final stage is the secondary instability of the streaky base state which leads to the onset of turbulent motion. Once turbulent spots are formed, their growth and merging to make up the fully-turbulent boundary layer is inevitable in zero-pressure-gradient flows.

Direct numerical simulations were performed in order to assess the influence of spanwise wall oscillation on the proceedings of bypass transition. Particular choice of the oscillation amplitude and frequency can weaken the disturbance field in the pre-transitional boundary layer. Specifically, the streaks that host the onset of secondary instability and the inception of turbulence spots are substantially reduced in amplitude with the application of the forcing. This behavior is due to a weakening in the lift-up mechanism.

Linear theory was applied in order to assess changes in the eigen-spectrum of the boundary layer due to the presence of wall oscillation. It was demonstrated that wall oscillation can indeed enhance shear sheltering. In general, the fraction of free-stream energy that penetrates the boundary layer diminishes with wall oscillation. In addition, while a simple Blasius boundary layer is susceptible to low-frequency disturbances from the free stream, the unsteady Blasius-Stokes flow is relatively more immune to these perturbations. Instead, disturbances whose wavenumber vector (k_x, k_z) is aligned with the shear (U', W') are more likely to penetrate the near-wall region (Hack & Zaki, 2012).

When the streaks are lower in amplitude, the flow is more stable and transition onset is delayed farther downstream than in the reference simulation. In addition, the transition length is longer in the streamwise direction in these cases. It should be cautioned, however, that varying the oscillation amplitude or frequency can also promote instability, and cause transition onset to move upstream, even ahead of the original transition location of the reference simulation.

References

Andersson, P., Berggren, M. & Henningson, D. S. 1999 Optimal disturbances and bypass transition in boundary layers. *Physics of Fluids* **11** (1), 134–150.

Andersson, P., Brandt, L., Bottaro, A. & Henningson, D. S. 2001 On the breakdown of boundary layer streaks. *Journal of Fluid Mechanics* **428**, 29–60.

Butler, K. M. & Farrell, B. F. 1992 Three-dimensional optimal perturbations in viscous shear flow. *Physics of Fluids A* **4** (8), 1637–1650.

Durbin, P. A. & Wu, X. 2007 Transition beneath vortical disturbances. *Annual Review of Fluid Mechanics* **39**, 107–128.

Hack, M. J. P. & Zaki, T. A. 2012 The continuous spectrum of time-harmonic shear layers. *Physics of Fluids* **24** (3), 034101.

Hack, M. J. P. & Zaki, T. A. 2014 Streak instabilities in boundary layers beneath free-stream turbulence. *Journal of Fluid Mechanics* **741**, 280–315.

Hunt, J. C. R. & Carruthers, D. J. 1990 Rapid distortion theory and the 'problems' of turbulence. *Journal of Fluid Mechanics* **212**, 497–532.

Hunt, J. C. R. & Durbin, P. A. 1999 Perturbed vortical layers and shear sheltering. *Fluid Dynamics Research* **464**.

Jacobs, R. G. & Durbin, P. A. 1998 Shear sheltering and the continuous spectrum of the Orr-Sommerfeld equation. *Physics of Fluids* **10** (8), 2006–2011.

Jacobs, R. G. & Durbin, P. A. 2001 Simulations of bypass transition. *Journal of Fluid Mechanics* **428**, 185–212.

Klebanoff, P. S. 1971 Effect of freestream turbulence on the laminar boundary layer. *Bull. Am. Phys. Soc* **16**, 1323.

Landahl, M. T. 1980 A note on an algebraic instability of inviscid parallel shear flows. *Journal of Fluid Mechanics* **98**, 243–251.

Liu, Y., Zaki, T. A. & Durbin, P. A. 2008*a* Boundary-layer transition by interaction of discrete and continuous modes. *Journal of Fluid Mechanics* **604**, 199–233.

Liu, Y., Zaki, T. A. & Durbin, P. A. 2008*b* Floquet analysis of secondary instability of boundary layers distorted by Klebanoff streaks and Tollmien–Schlichting waves. *Physics of Fluids* **20** (124102).

Mandal, A. C., Venkatakrishnan, L. & Dey, J. 2010 A study on boundary-layer transition induced by free-stream turbulence. *Journal of Fluid Mechanics* **660**, 114–146.

Matsubara, M. & Alfredsson, P. 2001 Disturbance growth in boundary layers subjected to free-stream turbulence. *Journal of Fluid Mechanics* **430**, 149–168.

Morkovin, M. V. & Obremski, H. J. 1969 Application of a quasi-steady stability model to periodic boundary-layer flows. *AIAA Journal* **7**, 1298–1301.

Nagarajan, S., Lele, S. K. & Ferziger, J. H. 2007 Leading-edge effects in bypass transition. *Journal of Fluid Mechanics* **572**, 471–504.

Nolan, K. P., Walsh, E. J. & McElligot, D. M. 2010 Quadrant analysis of a transitional boundary layer subject to free-stream turbulence. *Journal of Fluid Mechanics* **658**, 310–335.

Nolan, K. P. & Zaki, T. A. 2013 Conditional sampling of transitional boundary layers in pressure gradients. *Journal of Fluid Mechanics* **728**, 306–339.

Phillips, O. M. 1969 Shear-flow turbulence. *Annual Review of Fluid Mechanics* **1**, 145–146.

Quadrio, M., Ricco, P. & Viotti, C. 2009 Streamwise-Travelling Waves of Span-

wise Wall Velocity for Turbulent Drag Reduction. *Journal of Fluid Mechanics* **627**, 161–178.

Quadrio, M. & Sibilla, S. 2000 Numerical simulation of turbulent flow in a pipe oscillating around its axis. *JFM* **424**, 217.

Rogallo, R. S. 1981 Numerical experiments in homogeneous turbulence.

Schmid, P. J. & Henningson, D. S. 2000 *Stability and Transition in Shear Flows*. Springer, Berlin Heidelberg New York.

Vaughan, N. J. & Zaki, T. A. 2011 Stability of zero-pressure-gradient boundary layer distorted by unsteady Klebanoff streaks. *Journal of Fluid Mechanics* **681**, 116–153.

Von Kármán, T. 1948 Progress in the statistical theory of turbulence. *Proceedings of the National Academy of Sciences* **34**, 530–539.

Westin, K. J. A., Boiko, A. V., Klingmann, B. G. B., Kozlov, V. V. & Alfredsson, P. H. 1994 Experiments in a boundary layer subjected to free stream turbulence. Part 1. Boundary layer structure and receptivity. *Journal of Fluid Mechanics* **281**, 193–218.

Zaki, T. A. 2013 From streaks to spots and on to turbulence: Exploring the dynamics of boundary layer transition. *Flow, Turbulence and Combustion* **91**, 451–473.

Zaki, T. A. & Durbin, P. A. 2005 Mode interaction and the bypass route to transition. *Journal of Fluid Mechanics* **531**, 85–111.

Zaki, T. A. & Durbin, P. A. 2006 Continuous mode transition and the effects of pressure gradients. *Journal of Fluid Mechanics* **563**, 357–358.

Zaki, T. A. & Saha, S. 2009 On shear sheltering and the structure of vortical modes in single- and two-fluid boundary layers. *Journal of Fluid Mechanics* **626**, 111–147.